Multidisciplinary Cancer Investigation Original Article

January 2020, Volume 4, Issue 1

A Hierarchical Convolutional Neural Network Architecture for Brain Tumor Segmentation in 3D Brain Magnetic Resonance Imaging

Ayoub Adineh-vand[1], Gholamreza Karimi[1, *], Mozafar Khazaei[2]

[1] Electrical Engineering Department, Faculty of Engineering, Razi University, Kermanshah, Iran
[2] Fertility and Infertility Research Center, Health Technology Institute, Kermanshah University of Medical Sciences, Kermanshah, Iran

**Corresponding author: Gholamreza Karimi, Electrical Engineering, Faculty of Engineering, Razi University, Postal Code: 67149, Kermanshah, Iran. Tel: +988334343218, Fax: +988334343211, E-mail: ghkarimi@razi.ac.ir*

DOI:10.30699/acadpub.mci.4.1.5

Submitted: 9 November 2019
Revised: 12 December 2019
Accepted: 23 December 2019
e-Published: 1 January 2020

Keywords:
Brain Neoplasms
Nerve Net
Magnetic Resonance Imaging

Introduction: Brain tumors such as glioma are among the most aggressive lesions, which result in a very short life expectancy in patients. Image segmentation is highly essential in medical image analysis with applications, particularly in clinical practices to treat brain tumors. Accurate segmentation of magnetic resonance data is crucial for diagnostic purposes, planning surgical treatments, and also follow-up evaluation. Manual segmentation of a large volume of MRI data is a time-consuming endeavor, and this necessitates employing automatic segmentation techniques that are both accurate and reliable. However, the vast spatial and structural diversity of brain tissue poses serious challenges for this procedure. The current study proposed an automatic segmentation method based on convolutional neural networks (CNN), where weights of a pre-trained network were used as initial weights of neurons to prevent possible overfitting in the training phase.

Methods: As tumors were diverse in their shape, size, location, and overlapping with other tissue, it was decided to exploit a flexible and extremely efficient architecture tailored to glioblastoma. To remove some of the overlapping difficulties, morphological operators as a pre-processing step were utilized to strip the skull.

Results: The proposed CNN had a hierarchical architecture to exploit local and global contextual features to handle both high- and low-grade glioblastoma. To address biasing stem from the imbalance of tumor labels, dropout was employed and a stochastic pooling layer was proposed.

Conclusions: Experimental results reported on a dataset of 400 brain MR images suggested that the proposed method outperformed the currently published state-of-the-art approach in terms of various image quality assessment metrics and achieved magnitude fold speed-up.

INTRODUCTION

Image segmentation aims at partitioning images into homogeneous regions by employing spatial-spectral attributes of the image. A segmentation algorithm assigns a unique label to each pixel and defines segmented regions based on all pixels serving certain criteria. This task has an important

application in analyzing medical images, especially brain magnetic resonance images, to locate certain cells and tissue [1]. Magnetic resonance imaging (MRI) is known as one of the most accurate medical imaging techniques used in different medical diagnosing tasks such as brain tumors detection. Brain tumor segmentation in MR images plays a crucial role in the diagnosis and prediction of tumor growth to plan for an appropriate treatment schedule. While some tumors (e.g., meningioma) can be easily segmented, but glioblastoma or gliomas are surrounded by edema, usually scattered, appeared in very low contrast with variable shape and size, which makes the segmentation hard [2]. Therefore, segmentation methods used as thresholding [3], region growing [4], and clustering [5] lose their accuracy in extracting brain lesions. For the lesions that are inside the white matter, the severe overlaps between the white and gray matters result in low-resolution MR images and, consequently, failure of both non-parametric and multi-parametric classifiers in the detection task. The brain lesions appeared in the brain center can be mistakenly considered as the gray matter due to the intensity differences of the center and borders. The same problem exists on the brain surface, where the gray matter and cerebrospinal fluid are aligned together and may be considered as lesions [6]. To resolve this problem, many researchers use multimodal MR images in the diagnostic procedure [7]. The utilization of multimodal MR images, however, has four main problems: (1) obtaining such data due to the severity of the disease and the time limitation [8] is not always practical, (2) the multimodal MR collection is expensive, (3) redundant information leads to increasing the processing time and segmentation errors [3], and (4) multimodal MRI data are incompatible [9]. Several studies suggested applying image registration and enhancement algorithms before the segmentation task [10-12]. Meanwhile, semi-automatic feature descriptors can also be used in detection and segmention of brain lesions [2].

Designing in-domain task-oriented feature representations by learning a hierarchy of learning methods can be considered as a promising alternative approach. This sort of hierarchy is attainable by utilizing the convolutional neural network (CNN) [13]. The current study proposed a concurrent CNN architecture with a stochastic pooling scheme to efficiently handle dropout regularization. It was noticed that utilizing this method results in classifying pixels without considering the local dependencies and biasing during the learning phase. Therefore, it was proposed to use conditional random fields (CRFs) in conjunction with the transfer learning concept. A pre-trained model was used on Image Net [14] in which dependencies of labels were modeled considering the pixel-wise probability of initial weights. CRFs were utilized to model the pixel-wise probability as a form of cascaded and concurrent architecture. Although the computation of CRFs is always expensive, the efficiency of convolution operations makes the implementation of this approach significantly faster as compared with a regular CRF the proposed architecture was tested on two different datasets to show its performance. The first set contained 400 MR images acquired from real patients annotated by a neurosurgeon used for training and testing The second set, however, contained 15 simulated computed tomography (CT) images in GATE/GEANT4 [15]. These two sets had differences in terms of dimensionality (3D and 2D) as well as details of images. However, the second set (with much less complexity) was employed to validate the proposed method in terms of generalizability. In addition to accuracy, it was also reported that peak signal-to-noise ratio (PSNR), structural similarity index (SSIM), and feature similarity index (FSIM) [16-18] had a fair comparison with the state-of-the-art techniques.

The rest of this paper was organized as follows: Section 2 surveys the background of research. Details of the proposed method are described in Section 3. Section 4 provides the experimental results, and finally, the concluding remarks are given in Section 5.

The essential requirements of automatic brain MRI processing and classification systems are reducing subjective errors and processing time. Developing such a system is, however, still one of the most challenging tasks in pattern recognition community due to the complex texture of the brain. The design of a computer-aided diagnostics system to segment brain lesion includes the following steps [6]: (1) image acquisition, (2) pre-processing, (3) feature extraction, (4) normalization, (5) classification, (6) post-processing, and (7) evaluation. This design can be summarized as the flowchart in Figure 1.

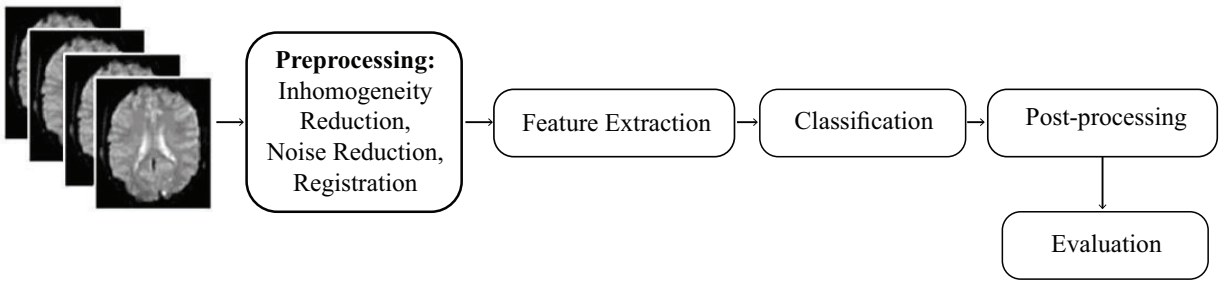

Figure 1: A Typical CAD System Used to Analyze Brain Lesions [6]

Data-driven, statistical, intelligent, and deformable models are four major categories of methods employed for brain lesion segmentation. The data-driven category contains thresholding, region growing, and hierarchical techniques [19]. Pachai et al., [20] proposed an automatic multi-resolution segmentation approach that used a pyramid data structure. The Gaussian pyramid decomposition was employed to keep an image at different resolutions. Restoring the shaded images and calculating their differences to original images resulted in creating a Laplace pyramid containing the most discriminative feature set. In the statistical-based methods, a probability density function is calculated. This category of methods can be further classified into parametric modeling and non-parametric probabilistic mapping. Anbeek et al., [21] used the k-nearest neighbor to determine the likelihood of a lesion in each voxel of a 3D MR image. The learning set consisted of five intensity coefficients of the Tx-w, T2-w, PD-w, PD-w, and FLAIR MR images fused with the (x, y, z) coordinates of each voxel. A probabilistic mapping was then generated based on the number of lesions present among the k-th neighbors. Eventually, using the threshold of this mapping, a binary segmentation was created. Guizard et al., [22] used a combination of the Gaussian model to detect lesions and tumors. They assumed that lesions' voxels had a different property from healthy tissue and considered them as the outlier of the intensity distribution. Warfield et al., [23] combined the statistical atlas of prior probabilities to distribute the designated structure in their proposed method for brain tumors segmentation. This atlas helped to discriminate brain tissue from the skull. They also used distance to the border of the brain in the feature set to separate the clusters. Freifeld et al., [24] proposed a constrained Gaussian mixture model that was a combination of several Gaussian distributions for each brain tissue. In this model, the brain tissue was constructed using T1-and T2-weighings, and Proton density (PD) modulations. The parameters of this model were measured using the EM method.

As a result, they were able to identify multiple sclerosis (MS) lesions as extra-Gaussian components and group them with other tissues to create a new class. Menze et al., [22] used the optimized EM algorithm in multimodal MR images to extract tumors in a different volume. Lao et al., [23] employed the combination of an SVM and stochastic Markov model in CRF to partition the brain tumor. The methods that use fuzzy logic or neural networks are classified as intelligent methods. Admasu et al., [24] introduced a fuzzy connectedness concept to improve the proposed artificial neural network method [25]. Shen et al., [26] employed fuzzy c-means (FCM) clustering to detect stroke lesions in single-spectral MR images. They calculated fuzzy membership functions and created a probabilistic mapping of the tissue using the SPM5 method. They used a threshold to segment lesions, where the incompatibility of the threshold between the pixel's intensity and the associated probability represented the target area. Deformable models consider volume estimation or growth/shrinkage of the estimated region. Metaxas et al., [27] presented a hybrid deformable method incorporating several deformable models such as the shape, texture integration, and graphical modeling. Cai et al., [28] used probabilistic mapping to separate all existing tissues, including edema, white matter, gray matter, and cerebrospinal fluid. This probabilistic mapping was also able to predict tumor growth simultaneously. Cuadra et

al., [29] modeled the prospect of lesion growth to separate large brain tumors in T1-weighted images. However, this semi-automatic method needs the cooperation of the user to select a voxel inside the tumor. Moreover, the user should have anatomical and biological structure knowledge of tumor growth to choose the voxel. Yang et al., [30] proposed to use a combination of deformable contours and FCM methods to segment white matters. However, this model was not comparable to other statistical methods in terms of performance criteria. Recent performances of deep learning methods in object recognition [14], multimodal data analysis [31], and biological image segmentation [32] increased their popularity among researches. Urban et al., [33] proposed a 3D CNN architecture for the multi-modal MRI glioma segmentation. They used extracted multimodal 3D patches from different brain MRI modalities as inputs to a CNN to predict the tissue label. Zikic et al., [34] developed an interpretation method in which a standard CNN architecture could handle different modalities of MR images to segment brain tumors. Havaei et al., [35] proposed a cascaded two-pathway CNN architecture that could handle both small- and large-sized patches at the same time. This cascaded CNN could process local details of the brain. Following this idea, a cascaded convolutional neural network was proposed in which dependencies of labels were modeled considering the pixel-wise probability of initial weights. CRFs were utilized to model the pixel-wise probability as a form of cascaded and concurrent architecture.

METHODS

The current study proposed a cascaded CNN architecture in which dependencies of labels were modeled considering the pixel-wise probability of initial weights. CRFs were utilized to model the pixel-wise probability as a form of cascaded and concurrent architecture. The main block of CNN is adapted to a pre-trained model [14], where a stack of convolutions creates a hierarchy of features to optimize initial weights during the training phase. It was realized that the presence of the skull and its premier (Figure 2a) increase the false positive rate. Therefore, these areas were removed by applying morphological operators. It was observed that using the dropout approach in the last pooling layer brought sparsity to feature space. Hence, a stochastic pooling method was proposed to resolve the sparsity and achieve the highest adaptation with the classification stage.

Preprocessing

In the preprocessing phase, morphological operators were employed to remove the skull from MR images. First, the largest connected component (i.e., brain) in the MR image was calculated by applying the gray-level histogram thresholding. The gray-level histogram has a binomial distribution, and minimizing the intensity variance discriminates the foreground (here, the brain tissue) from the background. Then, the dilation operator was applied using a 3×3 square structuring element. Dilation operator could keep the most important parts of the image, while filling the image holes. Finally, the supplementation of subtracting the input image from the expanded image could eliminate the skull texture (Figure 2b).

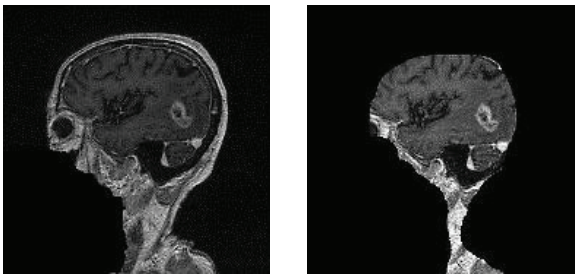

A) B)

Figure 2: Result of Applying Morphology to the Brain MR Image; (A) the Input Image and (B) the Brain Tissue After Skull Stripping

Proposed Tumor Segmentation Model

Since brain MR images in the dataset were 3D, the cutoff approach from the axial view was employed before giving them to the input of the proposed CNN model. Moreover, it was decided to test the proposed method on simulated CT images. Therefore, the cutoff was done to make the model consistent with the variety of inputs and generalizable. Indeed, the proposed model continuously processes each 2D axis image (cut) in a way that each pixel is associated with different weighting modes of T1 and T2. This method, similar to many CNN-based segmentation models [34, 35], predicts its pixel class by processing the M×M multimodal slice (X).

The main block of the pre-trained CNN architecture [14] is a stack of convolutions, which can form a hierarchy of features optimizing initial weights during the training phase. Each feature mapping is a

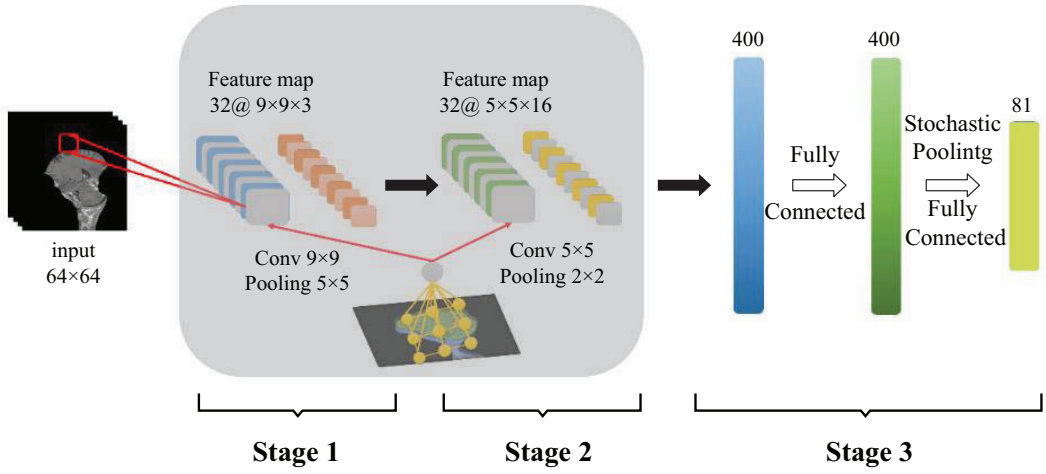

Figure 3: Computational Abstract Block of Features in a Convolutional Layer
The convolution of the input image is calculated with a set of kernels of 3×3 in size, followed by stochastic pooling.

topological structure made of extraction responses of a non-linear localized spatial property applied as a slider window, which further reinforces the bias of each neuron with a concurrent mapping schema. Figure 3 shows the calculation process of the topological mapping at three abstract stages of kernels convolution, nonlinear activation function, and conditional random fields as a concurrent reinforcement model. Equation 1 gives the latent representation of the k^{th} feature map for an input X in this architecture:

Equation 1: $h^k = \sigma(X \circledast W^k + b)$

where $\circledast$, b, W, and are the 2D convolution operator, the spread bias to the whole map, the sharing weights, and an activation function (in our experiments a hyperbolic tangent), respectively. The reconstruction is given by Equation 2.

Equation 2: $y = \sigma\left(\sum_{k \in H} h^k \circledast \tilde{w}^k + b\right)$

where H and are the set of latent feature maps, and the flip operation over both dimensions of the weights, respectively. The mean squared error (MSE) is the cost function or risk function, corresponding to the expected value of the squared error loss, which should be minimized over the training set as given by Equation 3.

Equation 3: $E = \frac{1}{2n}\sum_{i=1}^{n} (x_i - y_i)^2$

where n denotes the size of the training set. The gradient of the error function on the parameters is computed using the back-propagation algorithm (Equation 4).

Equation 4: $\frac{\partial E}{\partial W^k} = X \circledast \delta h^k + \tilde{h}^k \circledast \delta y$

where the hidden states and the reconstruction deltas are presented by h and y, respectively. To update the weights, stochastic gradient descent is applied.

In the max-pooling dropout strategy, the output is selected as the strongest activation multiplied by the retaining probability for completely connected layers. This strategy employs the whole network during the test phase regardless of the split compensate for outgoing weights. Therefore, the sparsity of feature space increases. To resolve the problem of sparsity and obtain small local deformations, a stochastic pooling scheme was proposed in which all non-maximal values in non-overlapping sub-regions are removed to cover sparsity over the hidden representation. The utilized CRF model directs the activation elements to intensify non-overlapping sub-regions. The proposed pooling scheme is formulated in Equation 5.

Equation 5: $pool_j = \sum_{i \in R_j} p_i a_i$

where a_i and p_i represent the activation elements in the i^{th} pooling region and the probabilities for each region, respectively. To calculate p_i, Equation 6 was employed.

Equation 6: $p_i = \frac{a_i}{\sum_{k \in R_j} a_k}$

The main difference between the proposed pooling method and the standard average pooling is the potential of weighting each region separately. Since the proposed probabilistic weighting approach calculates the average in the pooling regions, it can prevent L1 or L2 regularization over hidden units and reduce computational overhead. It was observed that using non-linear activation elements in convolutional kernels increased the discrimination of feature space. Following the idea of Goodfellow et al., [36], a nonlinear max-out was employed to create feature vectors. Since max-out features are associated with several kernels, each maximum dropout map (Z_s) is associated with K feature maps $\{O_s, O_{s+1}, \ldots, O_{s+K-1}\}$. Max-out features are responsible for maximizing O, which is calculated separately for each spatial location using Equation 7.

Equation 7:

$$Z_{s.i.j} = \max\{O_{s,i,j}, O_{s+1,i,j}, \ldots, O_{s+K-1,i,j}\}$$

where i and j are spatial positions. In this way, max-out features use the convex activation function to be shape consistent and dependent on the kernel values.

To intensify non-maximal values in non-overlapping sub-regions in this concurrent architecture, conditional random fields were employed. The computation of CRFs is similar to that of the one-shot mean-field inference (MFI) [37], where their dual potential functions in the kernel output kernel have the same weights. More precisely, the replication and repetition of MFI are performed in stages 1 and 2 of the proposed model, respectively.

Experiments

Datasets

In the current study, experiments were conducted on two datasets. The first set used for training and testing with the shares of 70-30, contains 400 3D brain MR images taken from 80 real patients. A neurosurgeon provided ground-truth for each patient. These 3D brain MR images had a degree of variation in their orientations, and there were 180 different points of view for each patient. T1- and T2-weight modalities existed for each brain co-registered image. Ground-truth brains came with three segmentation labels, including edema, non-tumor, and tumor. Figure 4 provides an example of the data and also the ground truth.

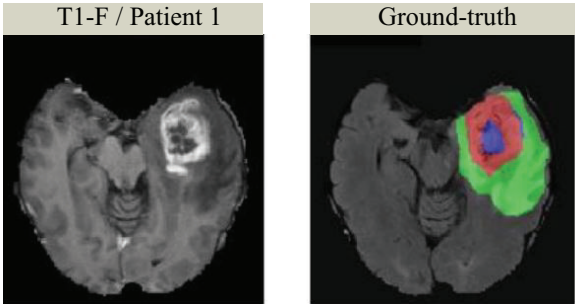

Figure 4: (A) MR T1-F Image Used as Input; (B) A Sample of Ground-Truth for Edema, Tumor, and Non-Tumor.

The second set contains 15 simulated CT images in GATE/GEANT4 [15]. Simulated CT images were employed to show the generalizability of the proposed deep learning model in handling data with different modalities. To construct the second set, the idea proposed in [42] was followed, which is created a phantom in the GATE/GEANT4 environment consisting of the skull, rib bone, and lung tissue surrounded by water. This phantom was then irradiated in a double-wedge way by a fan-beam X-ray. The X-ray spectrum was quantized into 13 intervals, ranged from 10 to 140 keV. To calculate the effective energy of each interval, the mean energy of each interval and its associated water attenuation coefficient [38] were used (Equation 8):

Equation 8: $$HU = \frac{\mu - \mu_w}{\mu_w} \times 1000$$

where is the attenuation coefficient, and is the water attenuation coefficient. A pixel-based attenuation matrix (PAM) was then created by applying the back-projection method. PAM was used to weight the value of HU and normalize photon flux. The phantom structure and positions of tissue are shown in Figure 5.

Figure 6 shows two outputs of the simulation. In order to visually distinguish differences between reconstructed CT images in different energy levels, an HSV color map was used.

RESULTS

To show the performance and accuracy of the proposed method, it was compared with the state-of-the-art. The average (AVG) and standard deviation (STD) of dice coefficient (DC), average symmetric surface distance (ASSD), and the Hausdorff distance (HD) were reported as quality evaluation metrics

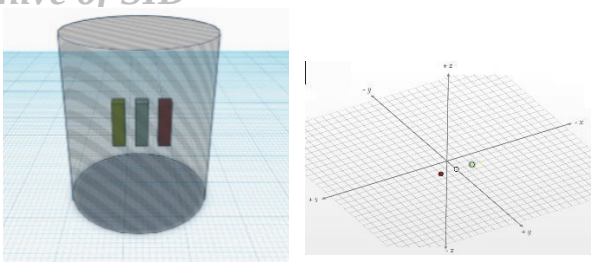

Figure 5: (A) Constructed Phantom in GATE; (B) Rib Bone (red), Lung (White), and Skull (Yellow) Tissue

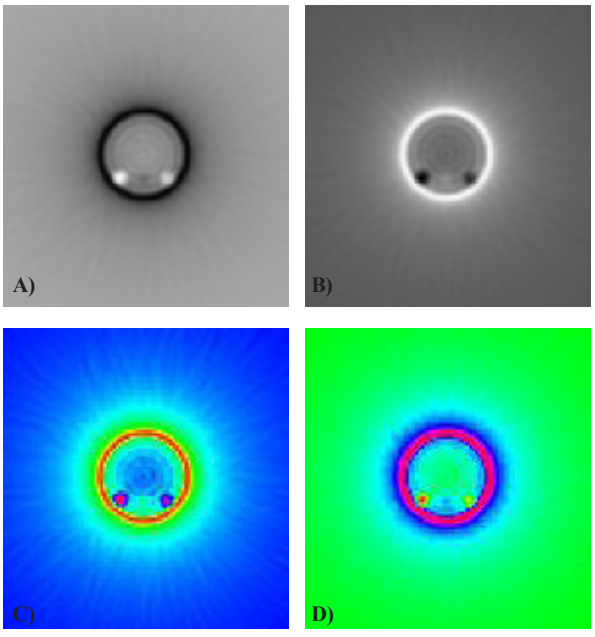

Figure 6: CT Images (200×200) in Energy Levels of (A) 35 and (B) 70 keV; HSV Color Map of Reconstructed CT Images in Energy Levels of (C) 35 and (D) 70 keV

[39] in Tables 1 (MR images) and 2 (reconstructed CT images). These values were obtained from a leave-one-out evaluation scheme. Furthermore, precision and recall were reported to discriminate over and under segmentation results, respectively. Two examples of segmentation results are shown in Figure 7.

PSNR, SSIM, and FSIM are other quantitative factors reported to show the performance of the proposed segmentation methods. The similarity of an image against a reference image is given by PSNR based on MSE of each pixel [18]. The SSIM compares the structure of the original and ground-truth images [40]. FSIM [16] is used to calculate the similarity between two images. Table 3 shows the superiority of the proposed method compared to the state-of-the-art in terms of PSNR, MSE, FSIM, and SSIM.

To have a better vision from the proposed architecture, the progression of forming features were visualized and the improvement was observed according to the Dice measure (Figure 8).

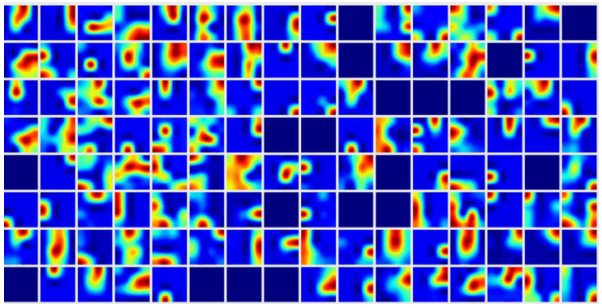

Figure 8: Feature Maps Generated in the Last Convolution Layer

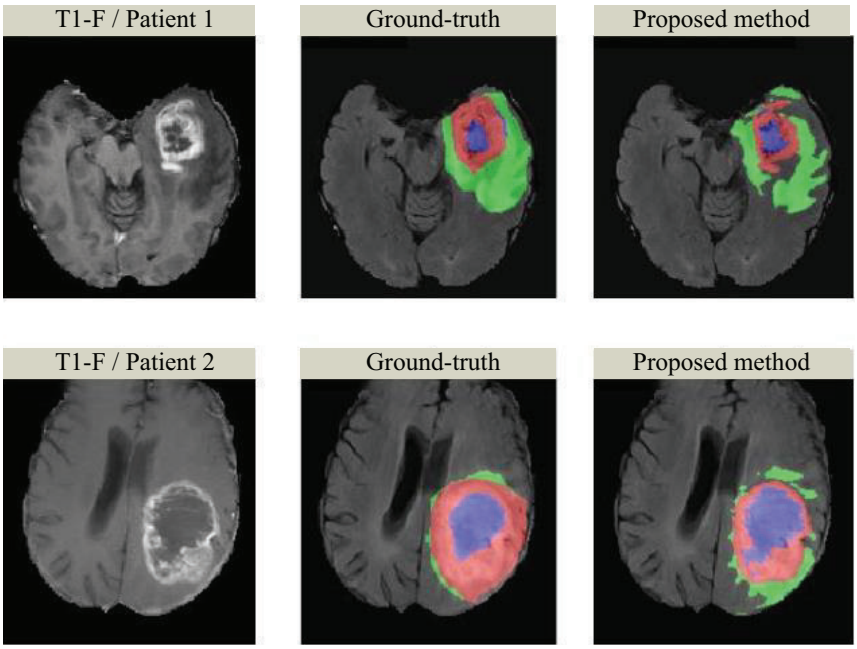

Figure 7: Segmentation Results of the Proposed Method for Two Patients.

Table 1: Comparison of the Proposed Method With the State-of-the-Art on the First Dataset

Method	ASSD		Dice		Hausdorff Distance		Precision		Recall	
	AVG	STD	AVG	STD	AVG	STD	AVG	STD	AVG	STD
Proposed	8.92	19.24	0.62	0.30	30.77	26.25	0.82	0.20	0.71	0.23
[41]	6.52	14.56	0.69	0.28	39.98	38.64	0.62	0.26	0.61	0.25
[42]	11.59	19.56	0.45	0.32	37.23	33.54	0.51	0.28	0.50	0.31
[34]	10.30	11.11	0.54	0.26	74.78	29.95	0.67	0.33	0.50	0.25
[35]	9.36	13.85	0.57	0.28	53.88	34.58	0.58	0.33	0.68	0.31

Table 2: Comparison of the Proposed Method With the State-of-the-Art on the Second Dataset

Method	ASSD		Dice		Hausdorff Distance		Precision		Recall	
	AVG	STD	AVG	STD	AVG	STD	AVG	STD	AVG	STD
Proposed	1.45	0.91	0.85	0.07	22.38	13.04	0.79	0.14	0.81	0.09
[41]	3.51	2.13	0.78	0.08	46.31	25.17	0.78	0.11	0.80	0.12
[42]	1.42	1.01	0.85	0.06	30.71	18.91	0.84	0.10	0.87	0.07
[34]	2.03	1.35	0.82	0.07	44.29	27.59	0.81	0.14	0.85	0.08

Table 3: Comparison of the Proposed Method With the State-of-the-Art Considering PSNR (dB), MSE, SSIM, and FSIM Measures [a]

Measure	PSNR				MSE				SSIM				FSIM			
Method	**P**	**[41]**	**[34]**	**[35]**	**P**	**[41]**	**[34]**	**[35]**	**P**	**[41]**	**[34]**	**[35]**	**P**	**[41]**	**[34]**	**[35]**
Image 1	24.65	24.64	24.64	24.64	2.22	2.22	2.23	2.23	0.94	0.90	0.92	0.94	0.89	0.72	0.77	0.88
Image 2	24.56	24.57	24.54	24.55	2.27	2.26	2.28	2.27	0.93	0.89	0.90	0.93	0.89	0.67	0.69	0.89
Image 3	24.62	24.58	24.58	24.57	2.24	2.26	2.26	2.27	0.94	0.86	0.88	0.94	0.90	0.66	0.70	0.90
Image 4	24.65	24.59	24.68	24.61	2.22	2.25	2.22	2.24	0.93	0.91	0.92	0.92	0.93	0.75	0.76	0.91
Image 5	24.52	24.51	24.47	24.46	2.29	2.29	2.31	2.32	0.93	0.90	0.89	0.93	0.92	0.71	0.68	0.90

[a] Note that results are tabulated for five test images, and "P" denotes to the proposed method.

DISCUSSION

The current study introduced an automatic brain lesion segmentation method based on a pre-trained CNN model on ImageNet in which the pooling layer was modified as a form of stochastic pooling scheme. It was proposed to use CRFs to model the pixel-wise probability as a form of cascaded and concurrent architecture to handle sparsity in feature vectors. Although the computation of CRFs is always expensive, the efficiency of convolution operations makes the implementation of this approach significantly faster as compared with a regular CRF. The proposed architecture was tested on two different data sets. The first set contained 400 MR images taken from real patients annotated by a neurosurgeon used for training and testing. The second set contained 15 simulated CT images in GATE/GEANT4. These two sets had differences in terms of dimensionality (3D and 2D) as well as modalities. The obtained results showed that the proposed method was accurate and generalizable compared to the state-of-the-art. In addition to accuracy, PSNR, SSIM, and FSIM were also reported. The proposed approach is suggested as a useful tool for both large-scale studies and clinical trials

ACKNOWLEDGEMENTS

The authors thank Dr. M. M. Dehshibi for his technical comments and also they would like to express their appreciation to the MFD co. for its support.

CONFLICT OF INTEREST

The authors have no conflicts of interest to declare.

ETHICS APPROVAL

The study was approved by the Ethical Committee of Med. Fanavaran Plus Co. (MFD).

REFERENCES

1. Balafar MA, Ramli AR, Saripan MI, Mashohor S. Review of brain MRI image segmentation methods. Artificial Intelligence Review. 2010;33(3):261-74. DOI: 10.1007/s10462-010-9155-0.
2. Menze BH, Jakab A, Bauer S, Kalpathy-Cramer J, Farahani K, Kirby J, et al. The multimodal brain tumor image segmentation benchmark (BRATS). IEEE transactions on medical imaging. 2014;34(10):1993-2024. DOI: 10.1109/TMI.2014.2377694 PMID: 25494501.
3. Lemieux L, Hagemann G, Krakow K, Woermann FG. Fast, accurate, and reproducible automatic segmentation of the brain in T1-weighted volume MRI data. Magnetic Resonance in Medicine: An Official Journal of the International Society for Magnetic Resonance in Medicine. 1999;42(1):127-35. DOI: 10.1002/(SICI)1522-2594(199907)42:1<127::AID-MRM17>3.0.CO;2-O.
4. Tang H, Wu E, Ma Q, Gallagher D, Perera G, Zhuang T. MRI brain image segmentation by multi-resolution edge detection and region selection. Computerized Medical Imaging and Graphics. 2000;24(6):349-57. DOI: 10.1016/S0895-6111(00)00037-9.
5. Zhang D-Q, Chen S-C. A novel kernelized fuzzy c-means algorithm with application in medical image segmentation. Artificial intelligence in medicine. 2004;32(1):37-50. DOI: 10.1016/j.artmed.2004.01.012 PMID: 15350623.
6. Mortazavi D, Kouzani AZ, Soltanian-Zadeh H. Segmentation of multiple sclerosis lesions in MR images: a review. Neuroradiology. 2012;54(4):299-320. DOI: 10.1007/s00234-011-0886-7 PMID: 21584674.
7. Clark MC, Hall LO, Goldgof DB, Velthuizen R, Murtagh FR, Silbiger MS. Automatic tumor segmentation using knowledge-based techniques. IEEE transactions on medical imaging. 1998;17(2):187-201. DOI: 10.1109/42.700731 PMID: 9688151.
8. Kabir Y, Dojat M, Scherrer B, Forbes F, Garbay C, editors. Multimodal MRI segmentation of ischemic stroke lesions. 2007 29th Annual International Conference of the IEEE Engineering in Medicine and Biology Society; 2007: IEEE. DOI: 10.1109/IEMBS.2007.4352610.
9. Roy S, Butman JA, Chan L, Pham DL, editors. TBI contusion segmentation from MRI using convolutional neural networks. 2018 IEEE 15th International Symposium on Biomedical Imaging (ISBI 2018); 2018: IEEE. DOI: 10.1109/ISBI.2018.8363545.
10. Zhang N, Ruan S, Lebonvallet S, Liao Q, Zhu Y. Kernel feature selection to fuse multi-spectral MRI images for brain tumor segmentation. Computer Vision and Image Understanding. 2011;115(2):256-69. DOI: 10.1016/j.cviu.2010.09.007.
11. Liu Z, Cao C, Ding S, Liu Z, Han T, Liu S. Towards clinical diagnosis: Automated stroke lesion segmentation on multi-spectral MR image using convolutional neural network. IEEE Access. 2018;6:57006-16. DOI: 10.1109/ACCESS.2018.2872939.
12. Dev KB, Jogi PS, Niyas S, Vinayagamani S, Kesavadas C, Rajan J. Automatic detection and localization of Focal Cortical Dysplasia lesions in MRI using fully convolutional neural network. Biomedical Signal Processing and Control. 2019;52:218-25. DOI: 10.1016/j.bspc.2019.04.024.
13. Bengio Y, Courville A, Vincent P. Representation learning: A review and new perspectives. IEEE transactions on pattern analysis and machine intelligence. 2013;35(8):1798-828. DOI: 10.1109/TPAMI.2013.50 PMID: 23787338.
14. Krizhevsky A, Sutskever I, Hinton GE, editors. Imagenet classification with deep convolutional neural networks. Advances in neural information processing systems; 2012.
15. Buvat I, Lazaro D. Monte Carlo simulations in emission tomography and GATE: An overview. Nuclear Instruments and Methods in Physics Research Section A: Accelerators, Spectrometers, Detectors and Associated Equipment. 2006;569(2):323-9. DOI: 10.1016/j.nima.2006.08.039.
16. Wang Z, Bovik AC, Sheikh HR, Simoncelli EP. Image quality assessment: from error visibility to structural similarity. IEEE transactions on image processing. 2004;13(4):600-12. DOI: 10.1109/TIP.2003.819861 PMID: 15376593.
17. Dehshibi MM, Sourizaei M, Fazlali M, Talaee O, Samadyar H, Shanbehzadeh J. A hybrid bio-inspired learning algorithm for image segmentation using multilevel thresholding. Multimedia Tools and Applications. 2017;76(14):15951-86. DOI: 10.1007/s11042-016-3891-3.
18. Yazdani D, Arabshahi A, Sepas-Moghaddam A, Dehshibi MM, editors. A multilevel thresholding method for image segmentation using a novel hybrid intelligent approach. 12th International Conference on Hybrid Intelligent Systems (HIS); 2012: IEEE. DOI: 10.1109/HIS.2012.6421323.
19. Wang L, Lai HM, Barker GJ, Miller DH, Tofts PS. Correction for variations in MRI scanner sensitivity in brain studies with histogram matching. Magnetic Resonance in Medicine. 1998;39(2):322-7. DOI: 10.1002/mrm.1910390222 PMID: 9469718.
20. Pachai C, Zhu Y, Grimaud J, Hermier M, Dromigny-Badin A, Boudraa A, et al. A pyramidal approach for automatic segmentation of multiple sclerosis lesions in brain MRI. Computerized Medical Imaging and Graphics. 1998;22(5):399-408. DOI: 10.1016/S0895-6111(98)00049-4.
21. Anbeek P, Vincken KL, Van Osch MJ, Bisschops RH, Van Der Grond J. Probabilistic segmentation of white matter lesions in MR imaging. NeuroImage. 2004;21(3):1037-44. DOI: 10.1016/j.neuroimage.2003.10.012 PMID: 15006671.
22. Menze BH, Van Leemput K, Lashkari D, Weber M-A, Ayache N, Golland P, editors. A generative model for brain tumor segmentation in multi-modal images. International Conference on Medical Image Computing and Computer-Assisted Intervention; 2010: Springer. DOI: 10.1007/978-3-642-15745-5_19.
23. Lao Z, Shen D, Liu D, Jawad AF, Melhem ER, Launer LJ, et al. Computer-assisted segmentation of white matter lesions in 3D MR images using support vector machine. Academic Radiology. 2008;15(3):300-13. DOI: 10.1016/j.acra.2007.10.012 PMID: 18280928.
24. Admasu F, Al-Zubi S, Toennies K, Bodammer N, Hinrichs H, editors. Segmentation of multiple sclerosis lesions from

MR brain images using the principles of fuzzy-connectedness and artificial neuron networks. Proceedings 2003 International Conference on Image Processing (Cat. No. 03CH37429); 2003: IEEE.

25. Udupa JK, Wei L, Samarasekera S, Miki Y, van Buchem MA, Grossman RI. Multiple sclerosis lesion quantification using fuzzy-connectedness principles. IEEE Transactions on Medical Imaging. 1997;16(5):598-609. DOI: 10.1109/42.640750 PMID: 9368115.
26. Shen S, Szameitat AJ, Sterr A. Detection of infarct lesions from single MRI modality using inconsistency between voxel intensity and spatial location—a 3-D automatic approach. IEEE Transactions on Information Technology in Biomedicine. 2008;12(4):532-40. DOI: 10.1109/TITB.2007.911310 PMID: 18632333.
27. Metaxas DN, Qian Z, Huang X, Huang R, Chen T, Axel L, editors. Hybrid deformable models for medical segmentation and registration. 9th International Conference on Control, Automation, Robotics and Vision; 2006: IEEE. DOI: 10.1109/ICARCV.2006.345077.
28. Cai H, Verma R, Ou Y, Lee S-k, Melhem ER, Davatzikos C, editors. Probabilistic segmentation of brain tumors based on multi-modality magnetic resonance images. 4th IEEE International Symposium on Biomedical Imaging: From Nano to Macro; 2007: IEEE. DOI: 10.1109/ISBI.2007.356923.
29. Bach Cuadra M, Pollo C, Bardera A, Cuisenaire O, Villemure J-G, Thiran J. Atlas-based segmentation of pathological MR brain images using a model of lesion growth. IEEE transactions on medical imaging. 2004;23(ARTICLE):1301-14. DOI: 10.1109/TMI.2004.834618 PMID: 15493697.
30. Yang F, Jiang T, Zhu W, Kruggel F, editors. White matter lesion segmentation from volumetric MR images. International Workshop on Medical Imaging and Virtual Reality; 2004: Springer. DOI: 10.1007/978-3-540-28626-4_14.
31. Dehshibi MM, Pons G, Baiani B, Masip D. VICSOM: VIsual Clues from Social Media for Psychological Assessment. International Journal of Computer Vision. 2019.
32. Ciresan D, Giusti A, Gambardella LM, Schmidhuber J, editors. Deep neural networks segment neuronal membranes in electron microscopy images. Advances in Neural Information Processing Systems; 2012.
33. Urban G, Bendszus M, Hamprecht F, Kleesiek J. Multi-modal brain tumor segmentation using deep convolutional neural networks. MICCAI BraTS (Brain Tumor Segmentation) Challenge. Proceedings, Winning Contribution. 2014:31-5.
34. Zikic D, Ioannou Y, Brown M, Criminisi A. Segmentation of brain tumor tissues with convolutional neural networks. Proceedings MICCAI-BRATS. 2014:36-9.
35. Havaei M, Davy A, Warde-Farley D, Biard A, Courville A, Bengio Y, et al. Brain tumor segmentation with deep neural networks. Medical Image Analysis. 2017;35:18-31. DOI: 10.1016/j.media.2016.05.004 PMID: 27310171.
36. Goodfellow IJ, Warde-Farley D, Lamblin P, Dumoulin V, Mirza M, Pascanu R, et al. Pylearn2: A Machine Learning Research Library. CoRR. 2013.
37. Xing EP, Jordan MI, Russell S, editors. A generalized mean field algorithm for variational inference in exponential families. Proceedings of the Nineteenth conference on Uncertainty in Artificial Intelligence; 2002: Morgan Kaufmann Publishers Inc.
38. Webster JG, Eren H. Measurement, instrumentation, and sensors handbook: spatial, mechanical, thermal, and radiation measurement: CRC press; 2016.
39. Ramin M, Sepas-Moghaddam A, Ahmadvand P, Dehshibi MM, editors. Counting the number of cells in immunocytochemical images using genetic algorithm. 12th International Conference on Hybrid Intelligent Systems (HIS); 2012: IEEE. DOI: 10.1109/HIS.2012.6421331.
40. Dehshibi MM, Alavi SM, editors. Generic Visual Recognition on Non-Uniform Distributions Based on AdaBoost Codebooks. Proceedings of the International Conference on Image Processing, Computer Vision, and Pattern Recognition (IPCV); 2011: Citeseer.
41. Warfield SK, Zou KH, Wells WM. Simultaneous truth and performance level estimation (STAPLE): an algorithm for the validation of image segmentation. IEEE transactions on medical imaging. 2004;23(7):903. DOI: 10.1109/TMI.2004.828354 PMID: 15250643.
42. Freifeld O, Greenspan H, Goldberger J. Multiple sclerosis lesion detection using constrained GMM and curve evolution. Journal of Biomedical Imaging. 2009;2009:14. DOI: 10.1155/2009/715124 PMID: 19756161.